*Structural Engineering and Mechanics, Vol. 39, No. 1 (2011) 1-20*
DOI: http://dx.doi.org/10.12989/sem.2011.39.1.001 

# Applications of Hilbert-Huang transform to structural damage detection

Dung-Jiang Chiou[1], Wen-Ko Hsu[1], Cheng-Wu Chen*[2,3], Chih-Min Hsieh[2], Jhy-Pyng Tang[1] and Wei-Ling Chiang[1]

*[1]Department of Civil Engineering, National Central University Jhung-li, Taoyuan, Taiwan, R.O.C.*
*[2]Institute of Maritime Information and Technology, National Kaohsiung Marine University, Kaohsiung 80543, Taiwan, R.O.C.*
*[3]Global Earth Observation and Data Analysis Center, National Cheng Kung University, Tainan, Taiwan 701, R.O.C.*

*(Received August 29, 2009, Accepted February 22, 2011)*

**Abstract.** This study investigates the feasibility of detecting structural damage using the HHT method. A damage detection index, the ratio of bandwidth (RB) is proposed. This index is highly correlated or approximately equal to the change of equivalent damping ratio for an intact structure incurring damage from strong ground motions. Based on an analysis of shaking table test data from benchmark models subjected to adjusted Kobe and El Centro earthquakes, the damage detection index is evaluated using the Hilbert-Huang Transform (HHT) and the Fast Fourier Transform (FFT) methods, respectively. Results indicate that, when the response of the structure is in the elastic region, the RB value only slightly changes in both the HHT and the FFT spectra. Additionally, RB values estimated from the HHT spectra vs. the PGA values change incrementally when the structure response is nonlinear i.e., member yielding occurs, but not in the RB curve from the FFT spectra. Moreover, the RB value of the top floor changes more than those from the other floors. Furthermore, structural damage is detected only when using the acceleration response data from the top floor. Therefore, the ratio of bandwidth RB estimated from the smoothed HHT spectra is an effective and sensitive damage index for detecting structural damage. Results of this study also demonstrate that the HHT is a powerful method in analyzing the nonlinear responses of steel structures to strong ground motions.

**Keywords:** damage detection index; HHT; inter-story drift; half-power bandwidth

## 1. Introduction

Structural health monitoring (SHM) has received considerable attention recently in structural engineering. While SHM attempts to detect structural damage in buildings, various approaches have been developed for detecting damage based on various methods (Doebling *et al.* 1996, Doebling *et al.* 1998, Salawu 1997, Black and Ventura 1998, Hou and Noori 1999, Hou *et al.* 2000, Sohn *et al.* 2003, Kim and Melhem 2004, Lanata and Del Grosso 2006, Bindhu *et al.* 2008, Zhang and Xu 2009, Sharma *et al.* 2010).

In data analysis and signal processing, Fast Fourier Transform (FFT) (Cooley and Tukey 1965) is

*Corresponding author, Ph.D., E-mail: chengwu@mail.nkmu.edu.tw

the conventional means of analyzing structural responses to obtain the damage detection parameters in the frequency domain. However, during strong ground motions, structural responses always exhibit nonlinear and non-stationary properties. Nevertheless, the significant phenomena of this response type cannot be displayed completely using the FFT method. Previous studies (Huang *et al.* 1998, Huang *et al*. 1999) proposed the empirical mode decomposition (EMD) and Hilbert-Huang transform (HHT) methods for non-stationary and nonlinear time series analysis. The HHT method has been extensively adopted in SHM to detect structural damage. Based on EMD and HHT (Yang and Lei 2000a) proposed the notion of identifying MDOF linear structural systems using the measured impulse response time history. The intrinsic mode functions (IMFs) decomposed by EMD are shown to be the modal responses. The Hilbert transform is then applied to each IMF in order to obtain the amplitude and phase angle to identify the physical mass, stiffness and proportional damping matrices of the structures. Later, (Yang and Lei 2000b) indicated that an IMF may involve the contribution of a complex conjugate pair of modes with a unique frequency and a damping ratio, referred to as the modal response. Additionally, all modal responses can be obtained from the IMFs. Each modal response is then decomposed in the frequency-time domain to yield an instantaneous phase angle and amplitude as functions of time when using the Hilbert transform to identify the non-proportional damping of the linear structure. Zhang *et al.* (2003) indicated that HHT-based Hilbert spectra can reveal the temporal-frequency energy distribution for motion recordings clearly. For MDOF systems, the normal modes are assumed to exist. Based on the Hilbert-Huang spectral analysis, (Yang *et al.* 2003a) proposed a linear least-square fit procedure to identify the natural frequency and damping ratio from the instantaneous amplitude and phase angle for each modal response. Frequently, all eigenvalues and eigenvectors of linear structures are complex (Yang *et al.* 2003b). An HHT based method has been extended further to identify general linear structures with complex modes using the free vibration response data polluted by noise. Although structural damage information is generally extracted from the measured data, recorded acceleration data in the damage location normally have a discontinuity relationship when the damage event occurs. Based on data analysis methods such as wavelet analysis, the damage time instants and locations can be detected (Hou and Noori 1999, Hou *et al.* 2000). Huang *et al*. (1998), Huang *et al.* (1999) showed the feasibility of using EMD and HHT to decompose a signal in the time-frequency domain more precisely than wavelet analysis can. Consequently, two methods were proposed based on EMD and HHT for detecting structural damage (Yang *et al.* 2004). The first method extracts damage spikes due to a sudden change of structural stiffness from the measured data. The damage time instants and damage locations could then be detected. The second method can detect the damage time instants and determine the natural frequencies and damping ratios of the structure before and after damage. These two proposed methods are then applied to a benchmark problem. According to those results, the proposed methods can detect damage and evaluate related structures efficiently. However, the stiffness and damping matrices cannot be identified quantitatively and the stiffness in each story is not assessed before and after damages. Therefore, the HHT method is further applied to phase I IASC-ASCE benchmark building to completely identify stiffness and damping coefficients before and after damage, respectively (Lin *et al.* 2005). The method consists of three steps: obtaining the cross-correlation functions from simulated ambient vibration data; identifying the modal parameters from the cross-correlation functions; and identifying the structural stiffness and damping from modal parameters. Then, each story unit prior to and after damage is compared in terms of stiffness to identify the damaged locations and severities. For structural components, these diagnostic techniques can be classified into modal-based methods, local diagnostic methods, non-parametric methods and time series/non-stationary methods (Pines and Salvino 2006). The procedure can be used to detect the structural defects through inspection of the time-frequency properties of the vibration signal by tracking the changes in these fundamental basis functions. As mentioned above, a new signal processing method, HHT (Huang *et al.* 1998, Huang *et al.* 1999), has been developed to analyze nonlinear and non-stationary data. A major feature of the method is the ability to extract IMFs that admit well-behaved Hilbert Transforms in magnitude and phase. This approach is adaptive and lends itself to any time series. When coupled with the Hilbert Transform, the IMFs yield instantaneous frequencies as functions of time that allow one to identify concisely the fundamental properties of vibration signals. The method is adopted in a previous study (Pines and Salvino 2006) to process the time series data from a variety of 1-D structures with and without structural damage to obtain the magnitude, phase and damping information. The location and extent of damage incurred by tracking the phase properties between successive degrees of freedom can be determined. Also, analysis results of the acceleration responses of the damaged structures clearly reveal the increases in damping.

Given that the HHT method often incurs the mode mixing problem when intermittency is involved in data, the new ensemble empirical mode decomposition (EEMD) method (Wu and Huang 2004) was proposed to overcome the intermittence phenomenon. The latest new HHT ensemble skills method has been utilized to analyze Tai-power Building stong-motion station records from 1994-2006 (Su *et al.* 2008). According to those results, the acceleration relations between the basement and the 27th story (top) are not proportional, even when the building maintains elasticity. A HHT-based damage detection method to two moment frames building is proposed (Raufi 2010). The result shows that the rotational response of nodes as the best option to detect damage of bending frame.

In reference to ATC-40 (ATC 1996) and FEMA-273 (Federal Emergency Management Agency 1997), the inter-story drift is normally used as a damage detection index. The yielding timing and damage location of the structural members are difficult to determine from the inter-story drift data. Additionally, the response displacement of each floor also cannot be obtained directly for an actual structure. A conventional mean of estimating response displacement is to integrate the measured acceleration data (Koichi and Ramasaomi 2003). However, the feasibility of the displacement estimated from the acceleration response data of a nonlinear structure, when using the integration method, is questionable. This study more closely examines this issue. Moreover, as is well known, the half-power bandwidth estimated from a frequency response curve Rd (Chopra 2001) is related to the damping ratio of a lightly-damped structure. Furthermore, the bandwidth normalized with the natural frequency increases with an increasing the structural damping ratio.

Instead of identifying the structural stiffness, natural frequencies and damping ratios of a structure before and after damage as mentioned above, this study proposes a simple structural damage detection index, in which the ratio of bandwidth (RB) based on the HHT method. RB denotes approximately the change of equivalent structural damping ratio in a structure if it has incurred damaged during an earthquake. Additionally, RB is estimated from the acceleration response curve Ra of the structure. The damage detection index RB is evaluated based on test data from the standard type benchmark A (NCREE-99-002) and benchmark B (NCREE-06-020), respectively, to show the sensitivity of the index. Benchmark A is a five-story, one-bay by one-bay, 1/2 scale steel building. Benchmark B is a three-story, one-bay by one-bay, real scale steel structure. During the tests, Benchmark A is subjected to the adjusted PGA (0.08 g, 0.1 g to 0.6 g) Kobe earthquake, while benchmark B is subjected to the adjusted PGA (0.1 g, 0.3 g to 1.2 g) El Centro earthquake. RB is evaluated based on the acceleration response data for each floor in these two models. The results of RB values using the FFT method demonstrate the performance of the HHT method.

## 2. Hilbert-Huang Transform (HHT)

The HHT, developed by Huang *et al*. (1998, 1999), consists of a two step-empirical mode decomposition (EMD) and the Hilbert spectral analysis (HSA). This section briefly summarizes the HHT principles and procedures. The detailed information can be found in the quoted references (Huang *et al.* 1998, 1999).

(1) Empirical Mode Decomposition (EMD):

The EMD method involves the extraction of the IMFs from a given time series. An IMF is a function that satisfies two conditions as follows:

(a) In a whole data set, the number of the extrema and the number of zero crossings must either be equal or differ at most by one.

(b) At any point, the mean value of the envelope defined by the local maxima and the envelope defined by the local minima is zero.

Once all IMFs are sifted from a given signal $x(t)$, it can be expressed as follows

$$x(t) = \sum_{i=1}^{n} c_i(t) + r_n(t) \tag{1}$$

where $n$ is the total number of the IMFs, and $r_n(t)$ denotes the final residue which represents the DC component (constant term) containing the overall trend of $x(t)$. The $c_i(t)$ are nearly orthogonal to each other and have nearly zero means.

(2) Hilbert Spectral Analysis:

For an arbitrary time series $X(t)$, the Hilbert transform, $Y(t)$, is defined as follows

$$Y(t) = \frac{1}{\pi} P \int_{-\infty}^{\infty} \frac{X(t')}{t-t'} dt' \tag{2}$$

where $P$ indicates the Cauchy principal value.

With this definition, $X(t)$ and $Y(t)$ can be combined to form the analytical signal $Z(t)$, as follows

$$Z(t) = X(t) + iY(t) = a(t)e^{i\theta(t)} \tag{3}$$

where

$$a(t) = [X^2(t) + Y^2(t)]^{1/2}, \quad \theta(t) = \left(\frac{Y(t)}{X(t)}\right)$$

From the polar coordinate expression of Eq. (3), the instantaneous frequency can be defined as

$$\omega(t) = \frac{d\theta(t)}{dt} \tag{4}$$

Applying the Hilbert transform to the $n$ IMFs components of $X(t)$ in Eq. (3), the data $X(t)$ can be written as follows

$$X(T) = \Re \sum_{j=1}^{n} a_j(t) e^{i\int \omega_j(t) dt} \tag{5}$$

where $\Re$ is the real part of the value.

Similar to the Fourier amplitude spectrum, the Hilbert amplitude spectrum $H(\omega, t)$ is the time-frequency distribution of amplitude. A measure of the total amplitude (or energy) contribution from each frequency value is the marginal spectrum $h(\omega)$. It represents the cumulated amplitude over the entire data span in a probabilistic sense. The marginal spectrum is obtained by integration the Hilbert spectrum over the time duration $T$

$$h(\omega) = \int_0^T H(\omega, t) dt \tag{6}$$

## 3. Damage detection of benchmark models

### 3.1 Damage detection index

The inter-story drift of a structure is generally used to represent the structural damage (ATC 1996, Federal Emergency Management Agency 1997), and increases when increasing the PGA value of the ground motions. Additionally, the natural frequency and the damping ratio of the structure subjected to strong ground motions change if any structural member is damaged. Both terms have been used as an index of damage detection (Doebling *et al.* 1996, Doebling *et al.* 1998). The change of the equivalent damping ratio of the structure before and after damage by earthquakes is the most obvious one among these indices. Therefore, this study derives the ratio of equivalent damping ratio RED, which refers to the occurrence and the extent of structural damaged caused by earthquakes.

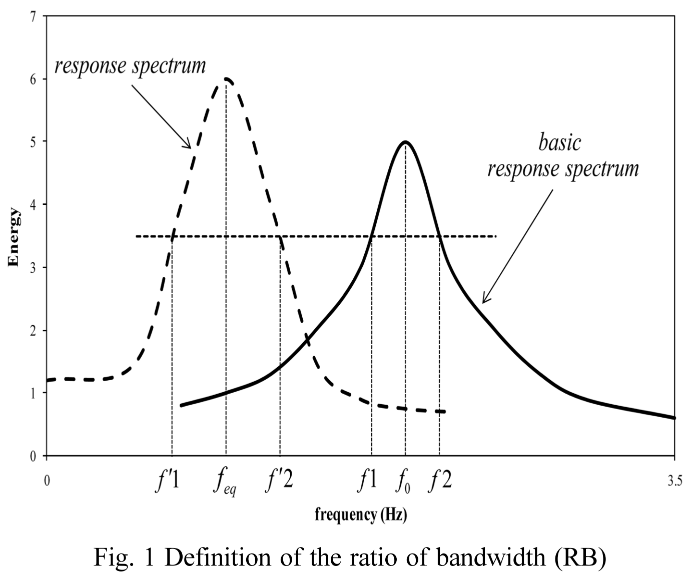


Fig. 1 Definition of the ratio of bandwidth (RB)

Initially, the ratio of bandwidth RB is defined as follows

$$RB = \frac{bandwidth\ of\ predominant\ frequency\ (f'2 - f'1)}{basic\ bandwidth\ of\ predominant\ frequency\ (f2 - f1)} \tag{7}$$

where the bandwidth $(f2-f1)$ or $(f'2-f'1)$ denotes the half-power bandwidth, as estimated from the acceleration frequency response curve Ra, as shown in Fig. 1. As is well known, the bandwidth estimated from a displacement frequency response curve Rd (Chopra 2001) is related to the equivalent damping ratio of a SDOF structure. Restated, the bandwidth increases with an increasing equivalent damping ratio, implying structural damage when the $\zeta < 0.05$. Therefore, the expansion of the half-power bandwidth represents, to some extent, an increase in structural damage. A similar finding can be obtained if the bandwidth is estimated from the acceleration frequency response curve Ra. Appendix A shows the derivation for the relationship of $(f2-f1)$ vs. damping ratio $\zeta$, as estimated from Ra.

For a lightly-damped SDOF structure, bandwidth $(f2-f1)$ is obtained from the elastic responses of the structure subjected to a moderate earthquake. The relationship of $(f2-f1)$ vs. damping ratio $\zeta_0$ of the structure can be expressed as follows

$$\zeta_0 = \frac{f2-f1}{2f_0} = \frac{f2-f1}{f2+f1} \tag{8}$$

where $f_0$ represents the natural frequency of the structure.

Similarly, the equivalent damping ratio $\zeta_{eq}$ estimated from another spectrum, as computed from the structural responses to a stronger ground motion, can be expressed as follows

$$\zeta_{eq} = \frac{f'2-f'1}{2f_{eq}} = \frac{f'2-f'1}{f'2+f'1} \tag{9}$$

where $f_{eq}$ represents the equivalent natural frequency of the structure.

By using Eq. (9) and Eq. (8), the relationship between the ratio of bandwidth RB and the ratio of equivalent damping ratio RED can be expressed as follows

$$RED = \frac{\zeta_{eq}}{\zeta_0} = \frac{f'2-f'1}{f2-f1} \times \frac{f_0}{f_{eq}} = RB \times \frac{f_0}{f_{eq}} \tag{10}$$

Since $f_0/f_{eq} \geqq 1$ and normally is approximately close to 1 except for a situation in which the attack ground motion is very strong, it is assumed that the value of $f_0/f_{eq} \cong 1$. Therefore, the ratio of bandwidth RB is highly correlated with or approximately equal to the ratio of equivalent damping ratio, and can be used as an index for damage detection. This assumption is discussed later.

For a MDOF structure to ground motions, the index RB can be estimated from the acceleration spectra analogous to that of a SDOF structure. According to Fig. 1, the solid line represents the spectrum of acceleration responses of the MDOF structure subjected to a moderate earthquake. The basic bandwidth of the predominant frequency, $(f2-f1)$, is obtained from the elastic responses of this spectrum. Another spectrum is then computed from the responses of the structure subjected to a stronger ground motion, as represented by the dashed line. The acceleration response is assumed to be the linear response with a larger damping ratio because for a steel structure to strong ground motions, only a small fraction of structural responses experience the plastic property. Along this line, the bandwidth of the predominant frequency, $(f'2-f'1)$, can be obtained following the definition of the half-power bandwidth as well. Next, the ratio of bandwidth RB can be estimated from the acceleration frequency response curve. Additionally, the values of $f_0/f_{eq}$ are checked using the numerical simulation results and the shaking table test data of two MDOF structures. Notably, since the bandwidth is difficult to estimate from an original structural response spectrum, the moving average skill (Chou 1975) is used to smooth the spectrum. Index RB is then evaluated from the smoothed curves.

### *3.2 Introduction to Benchmark steel structures*

The structures considered in this study are NCREE-99-002, standard type benchmark A (Loh and Huang 1999), and NCREE-06-020, standard type benchmark B (Lynch *et al.* 2006), steel frame models. These models were constructed by the National Center for Research on Earthquake

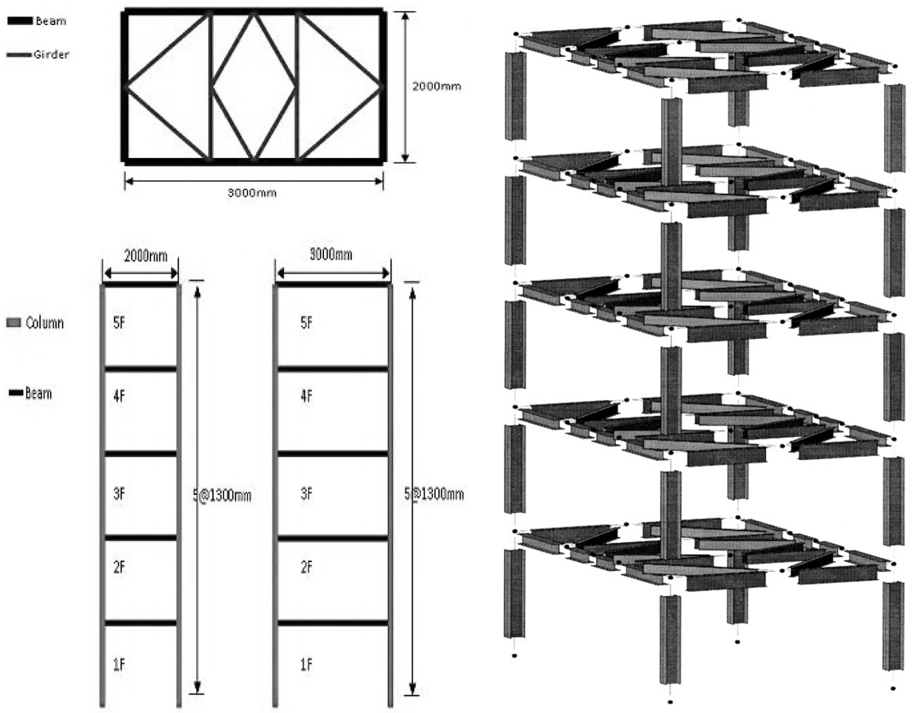


Fig. 2 Dimensions of standard benchmark A (NCREE-99-002)

Table 1 Benchmark A and benchmark B member sections

| Benchmark A | Direction-2m | Direction-3m |
|---|---|---|
| Column(1F~5F) | H125 × 125 × 6.5 × 9 | H125 × 125 × 6.5 × 9 |
| Beam(1F~5F) | H150 × 75 × 5 × 7 | H100 × 100 × 6 × 8 |
| Girder(1F~5F) | H100 × 50 × 5 × 7 | H100 × 50 × 5 × 7 |
| Benchmark B | Direction-2m | Direction-3m |
| Column(1F~3F) | H150 × 150 × 7 × 10 | H150 × 150 × 7 × 11 |
| Beam(1F~3F) | H150 × 150 × 7 × 10 | H150 × 150 × 7 × 11 |

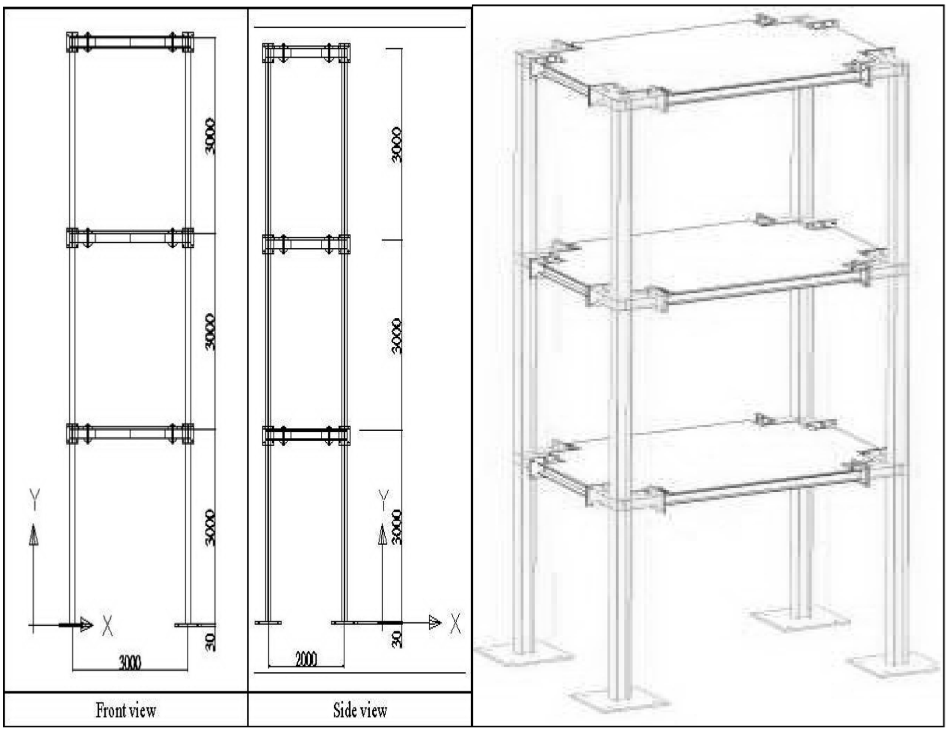


Fig. 3 Dimensions of standard benchmark B (NCREE-06-020)

Engineering (NCREE). Benchmark A is a five story, one-bay by one-bay, 1/2 scaled steel frame structure. It is 3 m × 2 m in plane and the height of each story is 1.3 m, as shown in Fig. 2. The steel floor is constructed using the girders of each story.

Table 1 lists the sections of each column, beam and girder. The beam-column joints are all bolt connected, and the support conditions are regarded as fully rigid supported. The lead blocks are attached to each floor symmetrically to present a nominal mass of 3664 kg. The acceleration meters and displacement meters are set at each floor in two directions (X-Y directions) to obtain global response data. Additionally, the first floor column is selected to set the acceleration meter, displacement meter, angular velocity meter and strain gauge to obtain the local member response data. The 1$^{st}$ modal frequency of the model in X direction (weak axis) is 1.43 Hz. Benchmark A is subjected to the adjusted PGA (0.08 g, 0.1 g …to 0.6 g) Kobe earthquakes along the X-axis in the tests. Benchmark B is a three story, one-bay by one-bay, real scale frame structure. The X-direction is 3 m, the Y-direction is 2 m and the height is 3 m of each story, as shown in Fig. 3.

A 25 mm thick steel plate is attached to each floor as the rigid floor and the mass of each floor is 6000 kg added symmetrically using lead blocks. The column and beam frame sections are made from A36 steel material, as shown in Table 1. The acceleration meters and displacement meters are also set at each floor in two directions (X-Y directions), and load cells are set at the bottom of 1F to gather the response data. The 1$^{st}$ and the 2$^{nd}$ modal frequencies of the model in X direction (strong axis) are 1.44 Hz and 4.52 Hz, respectively. Benchmark B is subjected to the adjusted PGA (0.1 g, 0.3 g … to 1.2 g) El Centro earthquakes along the X-axis.

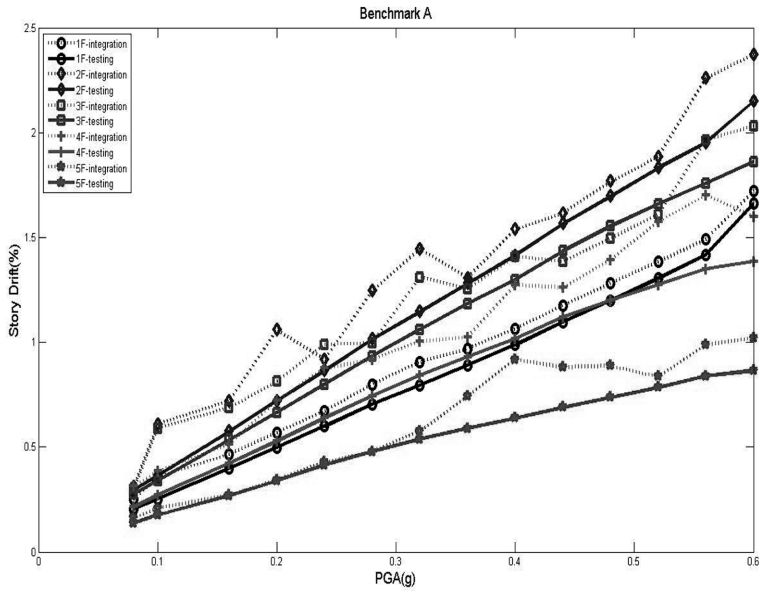


Fig. 4 Story drift vs. PGA curves from directly measured displacement responses and from integration of acceleration responses for benchmark A

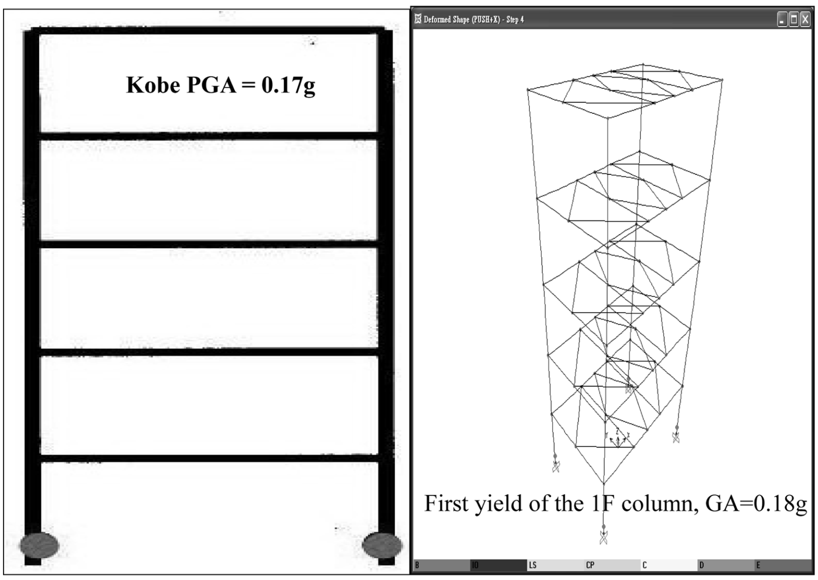


(a) (b)

Fig. 5 Yielding point of 1st floor column of benchmark A by: (a) Drain 2D program (NCREE-99-002) and (b) pushover analysis of SAP2000

### *3.3 Damage detection analysis*

As is well known, the inter-story drift is usually used to represent structural damage, like ATC-40

(ATC 1996) and FEMA 273 (Federal Emergency Management Agency 1997). Thus, this study discusses two objectives of the drift ratio based on the testing data of the benchmark models: (1) ability of the inter-story drift sensitivity to identify the damage location if a structural member has been yielded and (2) ability to represent the displacement responses based on the results of the acceleration integration method results. Fig. 4 shows the inter-story drift vs. PGA curves from directly measured displacement responses and from integration of acceleration responses for benchmark A. The inter-story drift increases with increasing PGA values; the maximum drift ratio is 2.2% at the 2$^{nd}$ floor. However, no noticeable change occurs in the curves from the directly measured data for various PGA values.

Therefore, the first yield of the structure can not be found from these curves. Fig. 5 shows the first yield PGA values from the analytical results for benchmark A. Fig. 5(a) shows the Drain 2D model results (NCREE-99-002, in Chinese). When the PGA = 0.17 g, the first yielding member of benchmark A is at the bottom of the 1$^{st}$ floor column. Meanwhile, Fig. 5(b) summarizes the pushover analysis results for the 3D SAP2000 model. Similar to the Drain 2D model results, the first yield member is also at the bottom of the 1$^{st}$ floor column and PGA = 0.18 g. These analytical results also coincide with the strain gage test data (NCREE-99-002, in Chinese), indicating that when the PGA = 0.2 g, the bottom of the 1$^{st}$ floor columns has already been yielded. From the above description, we can infer that, although the maximum inter-story drift occurs on the 2$^{nd}$ floor, the first yielding member in benchmark A is at the bottom of the 1$^{st}$ floor column, as shown in Fig. 4. Therefore, the inter-story drift is an inadequate damage detection index. Given the difficulty in measuring the displacement response of a real structure, the inter-story drift is computed using the acceleration integration method. Fig. 4 summarizes those results. In this Figure, the solid lines denote the inter-story drift from the measured displacement responses of each floor, while the dashed lines denote the results estimated from acceleration integration. Owing to the error of

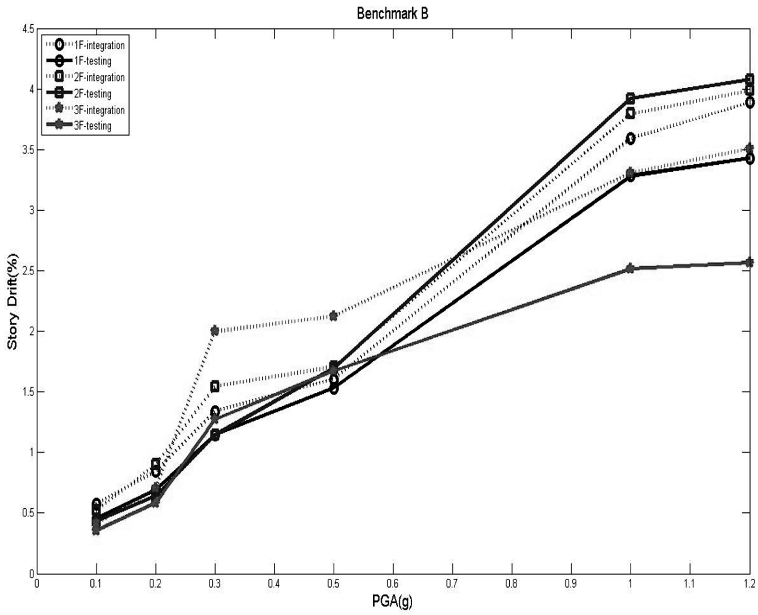


Fig. 6 Story drift vs. PGA curves from directly measured displacement responses and from integration of acceleration responses for benchmark B

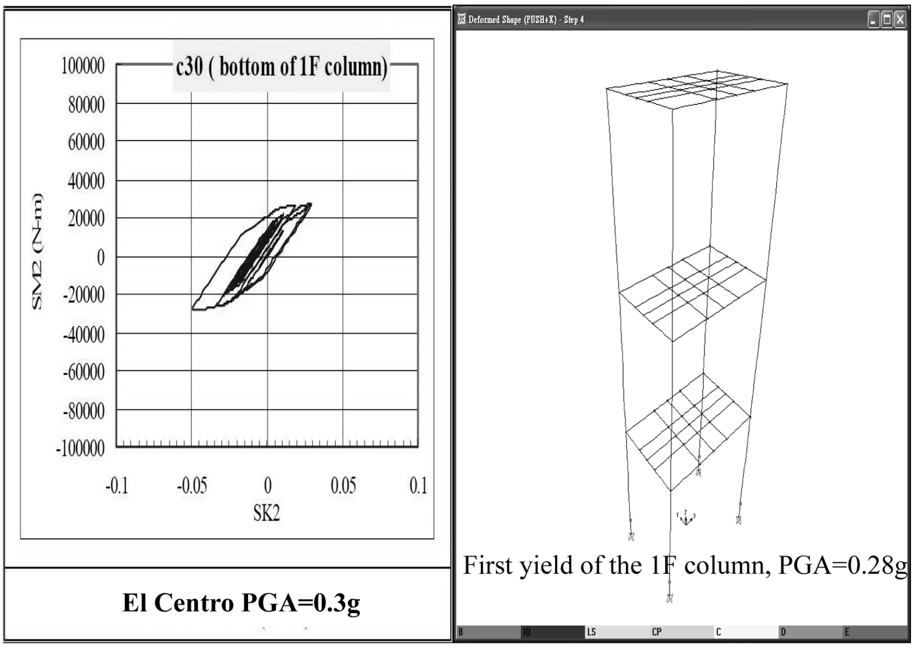


(a) (b)

Fig. 7 Yielding point of 1st floor column of benchmark B by (a) ABAQUS (NCREE-06-020) and (b) pushover analysis of SAP2000

integral procedure, the story drift is not monotonic increasing with PGA values observed from dashed lines. Results of the test data obviously differ from those of the integration method, especially when the nonlinear response occurs, i.e., the PGA value exceeds 0.2 g. Thus, the acceleration integration method may be inappropriate for estimating the nonlinear displacement responses of a structure. Fig. 6 displays the inter-story drift vs. PGA curves for the benchmark B, based on the directly measured displacements (denoted by solid lines) and the acceleration integration (denoted by dashed lines). Although the results of the integration method clearly deviate from the directly measured displacement responses, especially the 3F curve, the first yield of the structure can be identified from the abrupt changes of the slope of these curves. Fig. 7 shows a portion of the simulation results for benchmark B. Fig. 7(a) shows the ABAQUS model results (NCREE-06-020, in Chinese): the PGA = 0.3 g; and Fig. 7(b) the 3D SAP2000 pushover analysis: PGA = 0.28 g. Moreover, at the bottom of the 1st floor column is the first yielding member in benchmark B. The above analytical results indicate that, when PGA = 0.3 g, the bottom of the 1st floor columns has already been yielded. These results also coincide with the strain gage data (NCREE-06-020, in Chinese). Similar to the results of benchmark A, although the maximum inter-story drift occurs in the 2nd floor, the first yielding member in benchmark B is at the bottom of the 1st floor column, as shown in Fig. 7. Therefore, we conclude that the inter-story drift is insufficient to detect structural damage. Additionally, in both cases, results of the measured displacement responses significantly differ from those of the integration method. Thus, the acceleration integration method may be an inadequate means of estimating the nonlinear displacement responses.

Given the inability to use the inter-story drift to detect structural damage effectively, this study

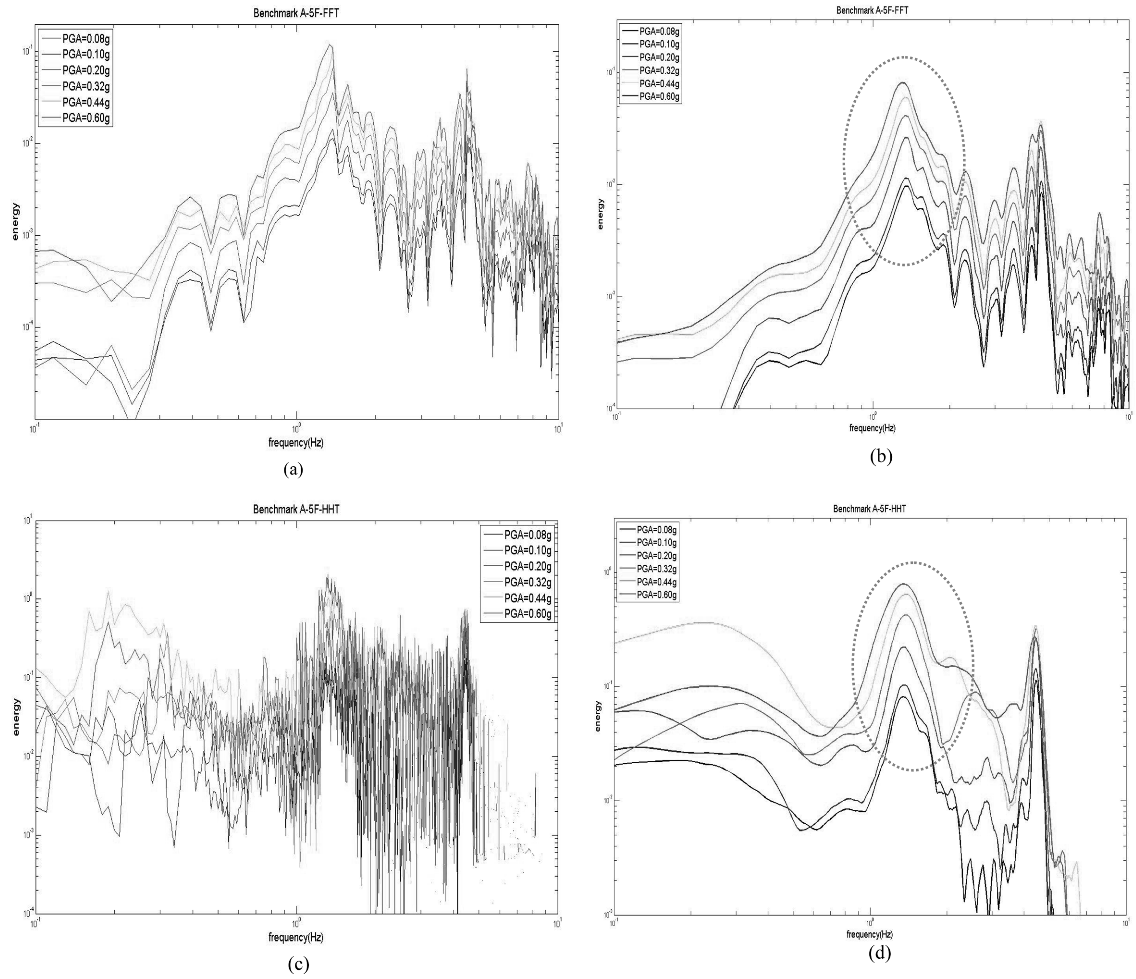


Fig. 8 Response spectra of the top floor for benchmark A (a) FFT spectra (b) smoothed FFT spectra (c) HHT spectra and (d) smoothed HHT spectra

proposes a new damage detection index, the ratio of bandwidth RB, to indicate the extent of damage in a structure from acceleration responses by using the HHT and FFT methods. Since the bandwidth is difficult to estimate from the original structural response spectrum, the spectrum is smoothed using the moving average method with span 3 (Chou 1975). Additionally, $\Delta f = 0.01\ Hz$ and each spectrum is smoothed ten times sequentially in this study. Fig. 8 shows the floor acceleration response spectra for benchmark A, while Figs. 8(a) and 8(b) display the FFT spectra for various adjusted Kobe earthquake intensities and the smoothed FFT spectra, respectively.

According to Figs. 8(a) and 8(b), the half-power bandwidth nearly maintains the same value and the change in bandwidth is observed clearly only in the case in which PGA = 0.6 g. Fig. 8(c) and Fig. 8(d) show the HHT spectra and the smoothed HHT spectra, respectively. According to these Figs, the half-power bandwidth increase with an increasing earthquake intensity. Figs. 9 and 10 show the smoothed FFT spectra and HHT spectra of each floor for various adjusted Kobe earthquake intensities, respectively. In Fig. 9, the changes in bandwidth for various intensities can

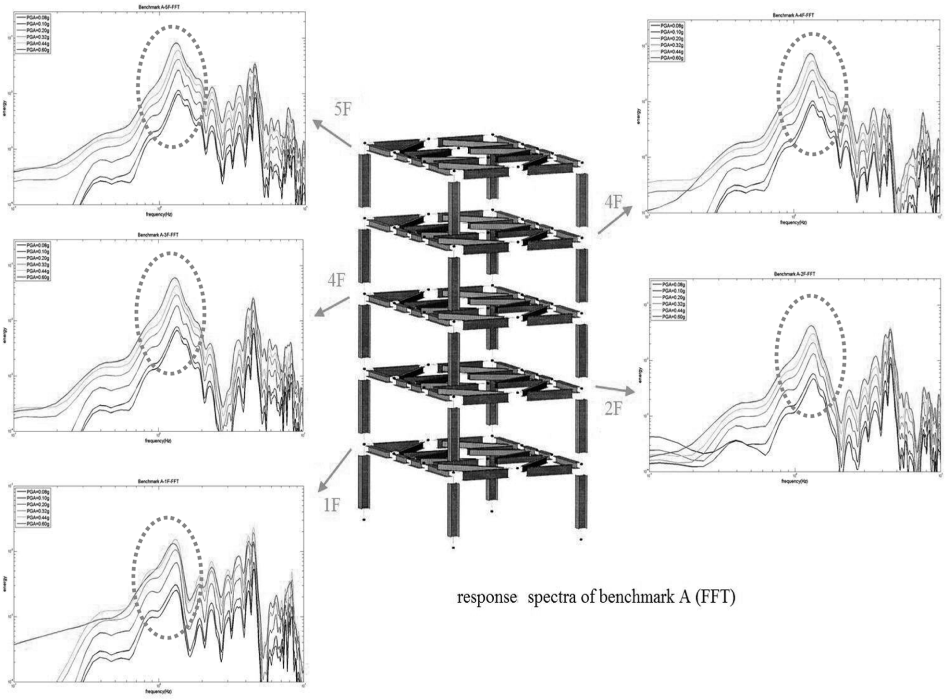


Fig. 9 Smoothed FFT spectra of each floor for benchmark A

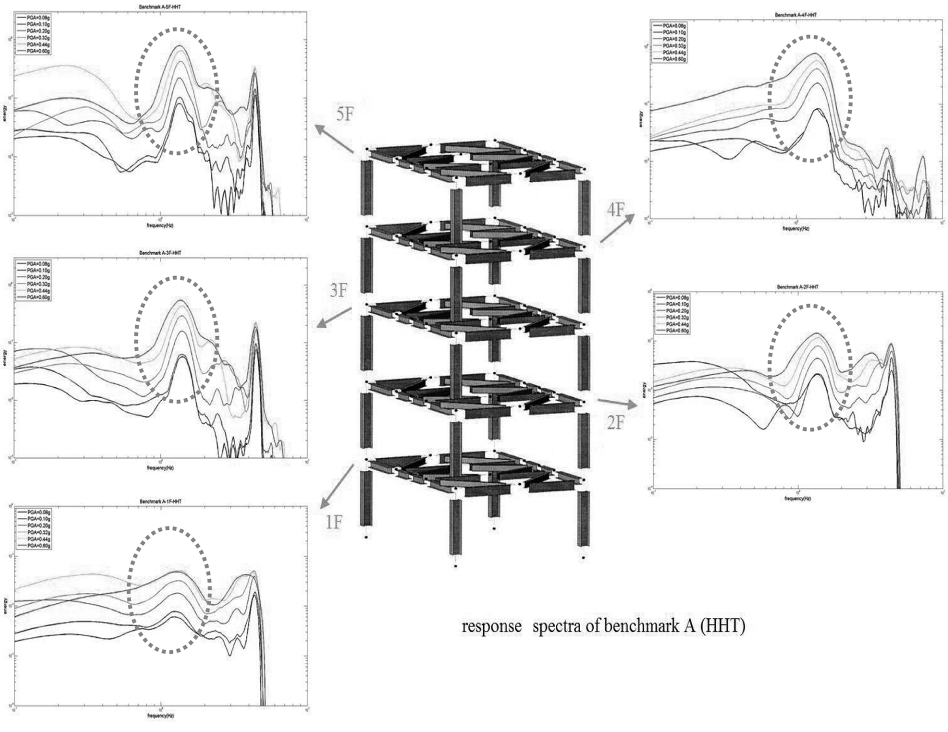


Fig. 10 Smoothed HHT spectra of each floor for benchmark A

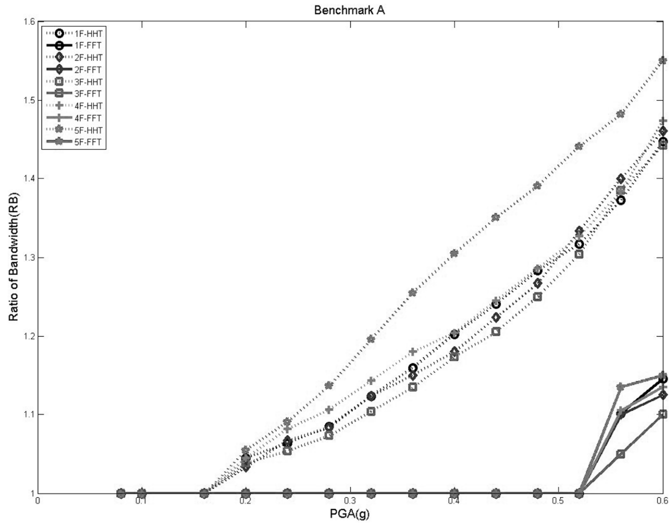


Fig. 11 RB vs. PGA curves for each floor from the FFT and HHT spectra for benchmark A

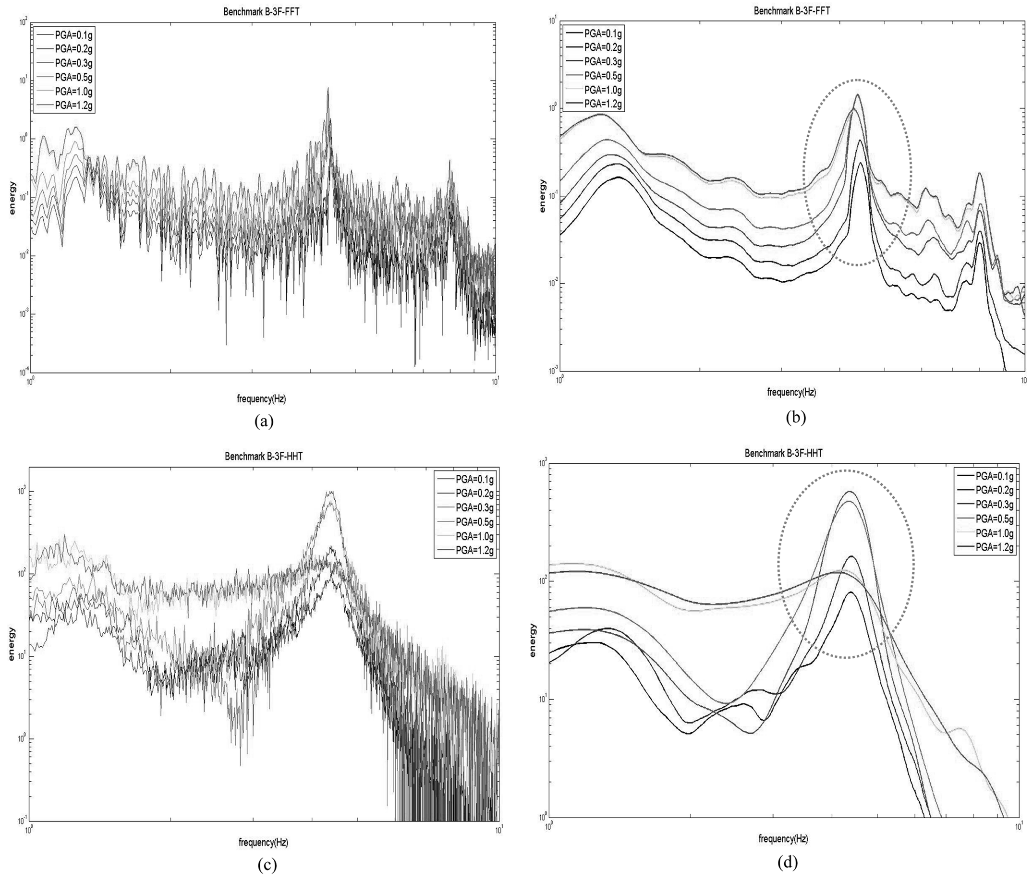


Fig. 12 Response spectra for the top floor for benchmark B: (a) FFT spectra (b) smoothed FFT spectra (c) HHT spectra and (d) smoothed HHT spectra

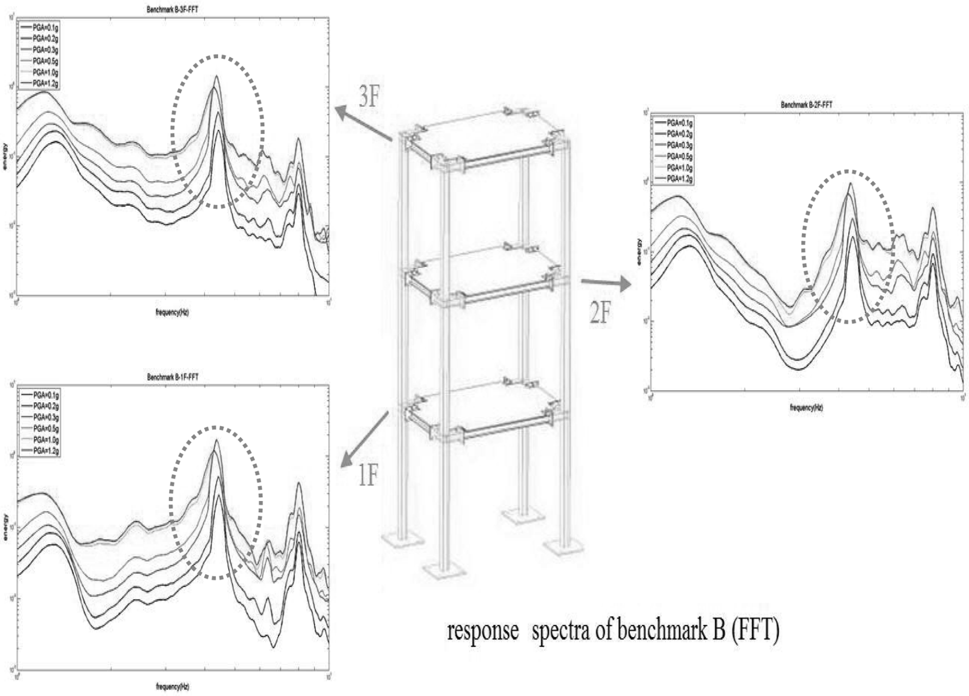


Fig 13 Smoothed FFT spectra for each floor for benchmark B

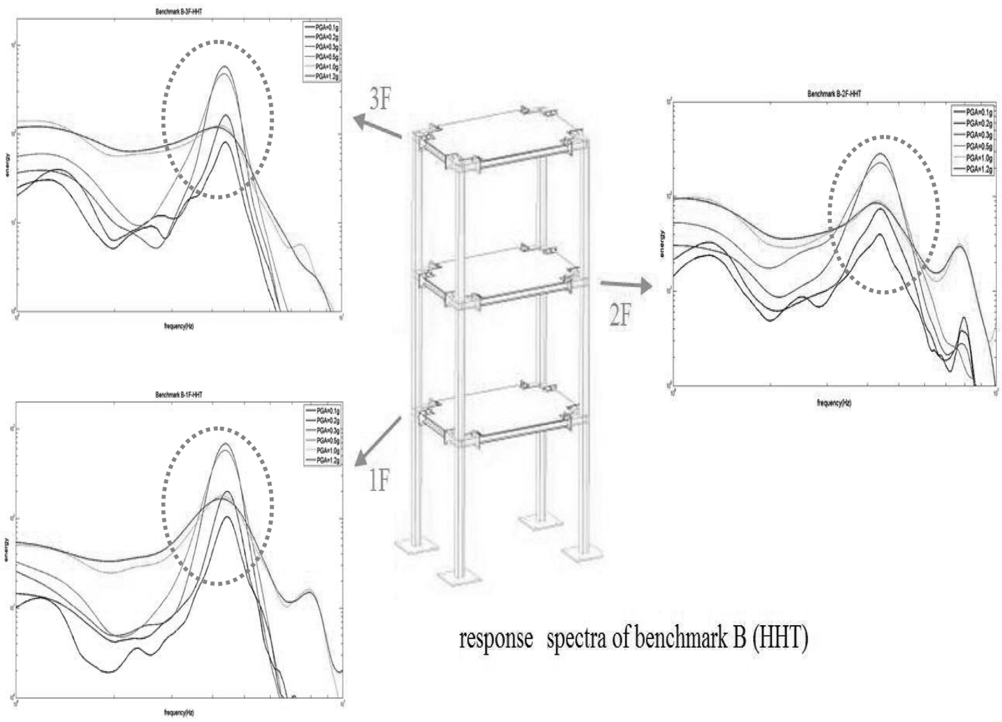


Fig 14 Smoothed HHT spectra for each floor for benchmark B

not be observed clearly in each floor. However, in Fig. 10, the changes in bandwidth for various intensities for each floor are found in the smoothed HHT spectra.

Fig. 11 presents the RB vs. PGA curves for each floor estimated from the FFT and HHT spectra for benchmark A. The change in RB is observed only when PGA is greater than 0.52 g in the FFT spectra and the maximum value of RB is only 1.15 in the 5th floor case. However, according to the HHT results, a situation in which RB increases with increasing PGA values is found results when PGA exceeds 0.2 g (the first column yield occurs). Nevertheless, the same phenomenon cannot be found in the FFT results. Additionally, the RB curve for the top floor is the highest one in Fig. 11. We can thus infer that the RB value from the HHT spectra is an effective and sensitive damage detection index. Notably, the bandwidths in Fig. 11 are estimated from the 1st mode of the X-axis for benchmark A.

Fig. 12 shows the spectra for the top floor acceleration for benchmark B. Figs. 12(a) and 12(b) show the FFT spectra for various adjusted El Centro earthquake intensities and the smoothed FFT spectra, respectively. Referring to Figs. 12(a) and 12(b), the predominant frequency shifts when the PGA value is greater than 1.0 g in the FFT spectra. Restated, the nonlinear behavior of benchmark B is clearly observed. However, the changes in bandwidth in the FFT spectra are not easily found, even in the case of PGA = 1.0 g. Similarly, the shift in the predominant frequency is also observed in the HHT spectra, as shown in Figs. 12(c) and 12(d). The bandwidth changes when increasing the PGA values in the HHT spectra, and can clearly be seen, especially when the PGA value exceeds 1.0 g.

Figs. 13 and 14 show the smoothed FFT spectra and the HHT spectra for each floor for various adjusted El Centro earthquake intensities, respectively. Fig. 13 indicates that the bandwidth changes only when the PGA value is sufficiently large. However, the changes in bandwidth for each floor are found in the smoothed HHT spectra for various earthquake intensities, especially in the top floor, as shown in Fig. 14.

Fig. 15 presents the RB vs. PGA curves for each floor from the smoothed FFT and HHT spectra for benchmark B. Notably, the bandwidths used in Fig. 15 are estimated from the 2nd mode of the

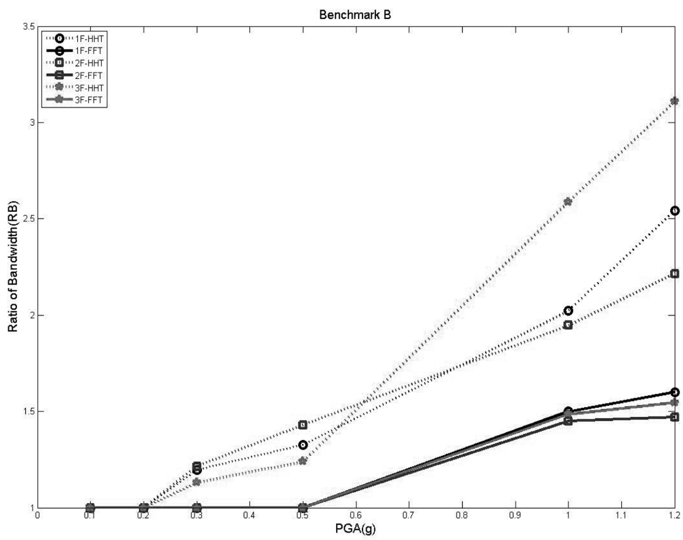


Fig. 15 RB vs. PGA curves for each floor from the FFT and HHT spectra for benchmark B

X-axis for benchmark B. The changes in RB are found only when the PGA value is greater than 0.5 g in the FFT spectra results; in addition, the maximum RB value is only 1.5. The RB values increase with increasing PGA values for each floor from the HHT spectra, resulting in a situation in which the PGA values are greater than 0.3 g. Additionally, the maximum RB value is 3.1 in the top floor. Although the change in RB is found in the smoothed HHT spectra when member yielding occurs, the same phenomenon is not found in the FFT spectra. Restated, the HHT method performs better than the FFT method in terms of detecting: the sensitivity of RB. Therefore, RB is a highly effective damage detection index for detecting structural damage induced by earthquakes if the HHT method is used.

## 4. Conclusions

This study proposes a damage detection index RB to detect the structural damage of the steel structure to strong ground motions. Experimental data of two benchmark models demonstrate the effectiveness of the HHT method in estimating the RB curves for structural damage detection. Results indicate that when the structural response is in the elastic region, the RB values only negligibly change in both the HHT and FFT spectra. However, the incremental change in RB vs. PGA from HHT method is clearly observed when the structural response is nonlinear i.e., member yielding has occurred. Restated, RB continuously increases with increasing PGA values if the structure experiences non-linear disruption. We conclude that the ratio of bandwidth RB estimated from the smoothed HHT spectra is an effective and sensitive damage detection index for detecting the structural damage of the steel structure to strong ground motions. The RB value of the top floor reveals a higher change value than that of the other floors. Therefore, structural damage can be detected using the acceleration response data from the top floor. Future studies should attempt to locate structural damage using the damage detection index, RB, in the HHT spectra.

## Acknowledgements

The author acknowledges the financial support from the National Science Council of Taiwan, R.O.C., under project number NSC 98-2221-E-366-006-MY2. The authors would also like to thank (1) Dr. Loh, the professor of civil engineering at National Taiwan University, for providing the test data for the benchmark models, (2) Dr. Norden E. Huang, the director of the Adaptive Data Analysis Research Center at National Central University, for his invaluable introduction of the HHT method, encouragement and advice for this study.

## References

Applied Technology Council (ATC) (1996), "Seismic evaluation and retrofit of concrete buildings", ATC 40, Redwood City, CA.

Bindhu, K.R., Jaya, K.P. and Manicka Selvam, V.K. (2008), "Seismic resistance of exterior beam-column joints with non-conventional confinement reinforcement detailing", *Struct. Eng. Mech.*, **30**(6), 733-761.

Black, C.J. and Ventura, C.E. (1998), "Blind test on damage detection of a steel frame structure", *Proceedings of* *the 16th International Modal Analysis Conference, Santa Barbara,* Society for Experimental Mechanics (SEM), Bethel, CT.

Chopra, A.K. (2001), "Earthquake dynamics of structures: theory and applications to earthquake engineering", Second Edition, Prentice Hall.

Chou, Y.L. (1975), *Statistical Analysis*, 2nd Edition, Holt Rinehart and Winston, New York.

Cooley, J.W. and Tukey, J.W. (1965), "An algorithm for the machine calculation of complex fourier series", *Math. Comput.*, **19**, 297-301.

Doebling, S.W., Farrar, C.R. and Prime. M.B. (1998), "A summary review of vibration based damage identification method", *Shock Vib. Dig.*, **30**(2), 91-105.

Doebling, S.W., Farrar, C.R., Prime, M.B. and Shevitz, D.W. (1996), "Damage identification and health monitoring of structural and mechanical system from changes in their characteristics: A literature review", Los Alamos National Laboratory Report LA-13070-MS.

Federal Emergency Management Agency (1997), "NEHRP guidelines for the seismic rehabilitation of buildings", FEMA-273, Building Seismic Safety Council, Washington D.C.

Hou, Z. and Noori, M. (1999), "Application of wavelet analysis For structural health monitoring", *Proceedings of the 2nd International Workshop on Structural Health Monitoring, Stanford Univ.,* Stanford, CA.

Hou, Z., Noori, M. and Amand, R. St. (2000), "Wavelet-based approach for structural damage detection", *J. Eng. Mech.*, **126**(7), 677-683.

Huang, N.E., Shen, Z. and Long, S.R. (1999), "A new view of nonlinear water waves: The Hilbert spectrum", *Annu. Rev. Fluid Mech.*, **31**, 417-457.

Huang, N.E., Shen, Z., Long, S.R., Wu, M.L.C., Shih, H.H., Zheng, Q.N., Yen, N.C., Tung, C.C. and Liu, H.H. (1998), "The empirical mode decomposition and the hilbert spectrum for nonlinear and non-stationary time series analysis", *Proc. R. Sec.115London A, The Royal Society*, 903-995.

Kim, H. and Melhem, H. (2004), "Damage detection of structures by wavelet analysis", *Eng. Struct.*, **26**(3), 347-62.

Koichi, K. and Ramasaomi, T. (2003), "A new acceleration integration method to develop a real-time residue seismic capacity evaluation system", *J. Struct. Constr. Eng.*, **569**, 119-126.

Lanata, F. and Del Grosso, A. (2006), "Damage detection and localization for continuous static monitoring of structures using a proper orthogonal decomposition of signals", *Smart Mater. Struct.*, **15**, 1811-1829.

Lin, S.L., Yang, J.N. and Zhou, L. (2005), "Damage identification of a benchmark building for structural health monitoring", *Smart Mater. Struct.*, **14**, S162-S169.

Loh, C.H. and Huang, C.C. (1999), "Damage Identification of multi-Story Steel Frames Using Neural Network", *Proceedings of Structural Health Monitoring,* Stanford Univ., 390-399.

Lynch, J.P., Wang, Y., Lu, K.C., Hou, T.C. and Loh, C.H. (2006), "Post-seismic damage assessment of steel structures instrumented with self-interrogating wireless sensors", *Proceedings of the 8th National Conference on Earthquake Engineering (8NCEE),* San Francisco, CA.

Pines, D. and Salvino, L. (2006), "Structural health monitoring using empirical mode decomposition and the Hilbert phase", *J. Sound Vib.*, **294**, 97-124.

Raufi, F. (2010), "Damage detection in moment frame building by using Hilbert-Huang transform", *Signal Processing Systems (ICSPS), 2nd International Conference,* July.

Salawu, O.S. (1997), "Detection of structural damage through changes in frequency: A review", *Eng Struct.*, **19**(9), 718-723.

Sharma, A., Redd, G.R., Eligehausen, R., Vaze, K.K., Ghosh, A.K. and Kushwaha, H.S. (2010), "Experiments on reinforced concrete beam-column joints under cyclic loads and evaluating their response by nonlinear static pushover analysis", *Struct. Eng. Mech.*, **35**(1), 99-117.

Sohn, H., Farrar, C.R., Hemez, F.M., Shunk, D.D., Stinemates, D.W. and Nadler, B.R. (2003), "A review of structural health monitoring literature: 1996-2001", Los Alamos National Laboratory Report LA-13976-MS.

Su, S.C., Huang, N.E. and Wen, K.L. (2008), "A new spectral representation of strong motion earthquake data: Hilbert spectral analysis of Taipower building station, 1994-2006", *Proceedings of the 5th International Conference on Urban Earthquake Engineering,* Tokyo, Japan.

Wu, Z. and Huang, N.E. (2004), "Ensemble empirical mode decomposition: a noise-assisted data analysis method", *Centre for Ocean-Land-Atmosphere Studies,* Tech. Rep.173.

Yang, J.N. and Lei, Y. (2000b), "Identification of civil structures with nonproportional damping", *Proc., SPIE*, **3988**, 284-294.
Yang, J.N. and Lei, Y. (2000a), "System identification of linear structures using Hilbert transform and empirical mode decomposition", *Proceedings of the 18th International Modal Analysis Conference: A Conference on Structural Dynamics*, Vol. 1, Society for Experimental Mech., Inc., Bethel, CT.
Yang, J.N., Lei, Y., Pan, S. and Huang, N. (2003a), "Identification of linear structures based on Hilbert-Huang transform. Part I: Normal modes", *Earthq. Eng. Struct. D.*, **32**(9), 1443-1467.
Yang, J.N., Lei, Y., Pan, S. and Huang, N. (2003b), "Identification of linear structures based on Hilbert-Huang transform. Part II: Complex modes", *Earthq. Eng. Struct. D.*, **32**(10), 1533-1554.
Yang, J.N., Lei, Y., Lin, S. and Huang N. (2004), "Hilbert-Huang based approach for structural damage detection", *J. Eng. Mech.-ASCE*, **130**(1), 85-95.
Zhang, J. and Xu, S.Y. (2009), "Seismic response simulations of bridges considering shear-flexural interaction of columns", *Struct. Eng. Mech.*, **31**(5), 545-566.
Zhang, R. R.C., Ma, S., Safak, E. and hartzell, S. (2003), "Hilbert-Huang transform analysis of dynamic and earthquake motion recordings", *J. Eng. Mech.-ASCE,* **129**(8), 861-875.

## Appendix A: Derivation for the relationship of ($f2 - f1$) vs. damping ratio $\zeta$, estimated from Ra

While referring to Chopra (2001), equating $R_d$ from Eq. (1.1) and $1/\sqrt{2}$ times the resonant amplitude of $R_d$ given by Eq. (1.2), by definition, the forcing frequencies $\omega_1$ and $\omega_2$ satisfy the following condition

$$R_d = \frac{u_0}{(u_{st})_0} = \frac{1}{\sqrt{[1-(\omega/\omega_n)^2]^2 + [2\zeta(\omega/\omega_n)]^2}} \tag{1.1}$$

$$R_d = \frac{1}{\sqrt{2}} \times \frac{1}{2\zeta\sqrt{1-\zeta^2}}, \quad R_a = \frac{1}{\sqrt{2}} \times \frac{1}{2\zeta\sqrt{1-\zeta^2}} \tag{1.2}$$

$$\frac{1}{\sqrt{[1-(\omega/\omega_n)^2]^2 + [2\zeta(\omega/\omega_n)]^2}} = \frac{1}{\sqrt{2}} \times \frac{1}{2\zeta\sqrt{1-\zeta^2}} \tag{a}$$

From Eq. (1.3), the *acceleration response factor* $R_a$ is related to $R_d$ by

$$R_a = \left(\frac{\omega}{\omega_n}\right)^2 \times R_d \tag{1.3}$$

Therefore, $R_a$ can be expressed as

$$\left(\frac{\omega}{\omega_n}\right)^2 \times \frac{1}{\sqrt{[1-(\omega/\omega_n)^2]^2 + [2\zeta(\omega/\omega_n)]^2}} = \frac{1}{\sqrt{2}} \times \frac{1}{2\zeta\sqrt{1-\zeta^2}} \tag{b}$$

Inverting both sides, squaring them, and rearranging the terms give

$$\left(\frac{\omega}{\omega_n}\right)^4 - \left(\frac{2-4\zeta^2}{1-8\zeta^2+8\zeta^4}\right)\left(\frac{\omega}{\omega_n}\right)^2 + \frac{1}{1-8\zeta^2+8\zeta^4} = 0 \tag{c}$$

Equation (c) is a quadratic equation in $(\omega/\omega_n)^2$, the roots of which are

$$\left(\frac{\omega}{\omega_n}\right)^2 = \frac{1-2\zeta^2}{1-8\zeta^2+8\zeta^4} \pm \frac{2\sqrt{(\zeta^2-\zeta^4)}}{1-8\zeta^2+8\zeta^4} \tag{d}$$

where the positive sign gives a larger root $\omega_2$ and the negative sign corresponds to a smaller root $\omega_1$.

$$\left(\frac{\omega}{\omega_n}\right) = \sqrt{\frac{1-2\zeta^2 \pm 2\sqrt{(\zeta^2-\zeta^4)}}{1-8\zeta^2+8\zeta^4}} \tag{e}$$

For the small damping ratios representative of practical structures, the term containing $\zeta^4$ and $\zeta^2$ can be dropped and

$$\left(\frac{\omega}{\omega_n}\right) \simeq \sqrt{1 \pm 2\zeta} \tag{f}$$

Taking only the first term in the Taylor series expansion of the right side gives

$$\left(\frac{\omega}{\omega_n}\right) \simeq 1 \pm \zeta \tag{g}$$

Subtracting the smaller root from the larger one gives

$$\frac{\omega_2-\omega_1}{\omega_n} = 2\zeta \quad \text{or} \quad \frac{f_2-f_1}{f_n} = 2\zeta \tag{h}$$

Therefore, the *ratio of bandwidth*, RB can be expressed as

$$RB = \frac{f_2'-f_1'}{f_2-f_1} = \frac{f_{eq}}{f_0} \times \frac{\zeta_{eq}}{\zeta_0} \tag{i}$$